Chapter-4

Synthesis of Graphene Oxide and Reduce Graphene Oxide from Vacuum Gas Oil Derived Graphitic Carbon

4.1 Introduction

In modern petroleum refining, the characterization of intermediate feedstocks plays a pivotal role in optimizing product yields, improving process efficiency, and reducing operational costs. Among the various properties used to evaluate petroleum fractions, carbon residue—particularly measured as Micro Carbon Residue (MCR) or Conradson Carbon Residue (CCR)—serves as a critical parameter for understanding a material's thermal stability and coke-forming tendency under high-temperature conditions [1]. This residue represents the amount of carbonaceous material left after the thermal decomposition of a petroleum sample in an inert atmosphere, and is measured through standardized methods such as ASTM D4530 [2]. While simple in concept, carbon residue measurements provide deep insight into the composition of complex hydrocarbon streams and their behaviour in downstream refining processes.

One such stream is Vacuum Gas Oil (VGO), a high-boiling intermediate product obtained from the vacuum distillation of crude oil. VGO is a vital feedstock for various upgrading processes, particularly Fluid Catalytic Cracking (FCC), where it is transformed into lighter, more valuable products like gasoline, diesel, and olefins [3]. The performance of VGO in these processes is heavily influenced by its chemical composition, particularly the presence of heavy aromatic structures, asphaltenes, and resins, which contribute directly to the carbon residue value [4]. Although VGO is considered cleaner compared to heavier residual fractions, variations in its carbon residue content can significantly affect operational outcomes.

The carbon residue value of VGO serves as a key quality indicator, especially in the context of catalytic cracking operations, where coke formation is a major concern. Coke deposits

on the catalyst surface during FCC not only deactivates active sites but also reduces conversion efficiency and necessitates frequent catalyst regeneration cycles [5,6]. High carbon residue in VGO correlates with increased coke production, leading to lower yields of desirable products and increased energy consumption [7]. For this reason, monitoring and controlling the carbon residue in VGO is essential for refineries aiming to enhance profitability, extend catalyst life, and reduce the environmental impact of their operations.

4.1.1 Graphene

Graphene, a single layer of carbon atoms tightly packed in a two-dimensional honeycomb lattice, has garnered unprecedented attention since its successful isolation in 2004. This one-atom-thick material is not only the thinnest known substance but also one of the strongest, most conductive, and most transparent materials ever discovered [8,9]. Its remarkable suite of properties—including high electron mobility, superior thermal conductivity, exceptional mechanical strength, and optical transparency—has led researchers to consider it a "wonder material" of the 21st century. These characteristics position graphene as a revolutionary material across a wide spectrum of technological domains, including nanoelectronics, energy storage, biomedicine, flexible displays, and advanced composites [10].

Despite its enormous potential, the transition of graphene from laboratory discovery to widespread commercial application remains hindered by challenges in its scalable and cost-effective production. Multiple synthesis routes—such as chemical vapor deposition (CVD), epitaxial growth on silicon carbide, chemical reduction of graphene oxide, and liquid-phase exfoliation—have been developed to obtain graphene [11]. However, many of these methods involve high temperatures, toxic chemicals, or complex procedures that limit their industrial viability.

Among these techniques, direct exfoliation of graphite has emerged as one of the most promising, scalable, and relatively eco-friendly methods for producing high-quality graphene in bulk. Graphite, the naturally occurring parent material of graphene, consists of multiple layers of graphene held together by weak van der Waals forces. These

interlayer forces allow the graphite to be mechanically or chemically exfoliated into individual graphene sheets under appropriate conditions [12]. This method not only offers a practical pathway for large-scale graphene production but also retains much of the pristine quality of the graphene layers, making it suitable for a wide range of applications.

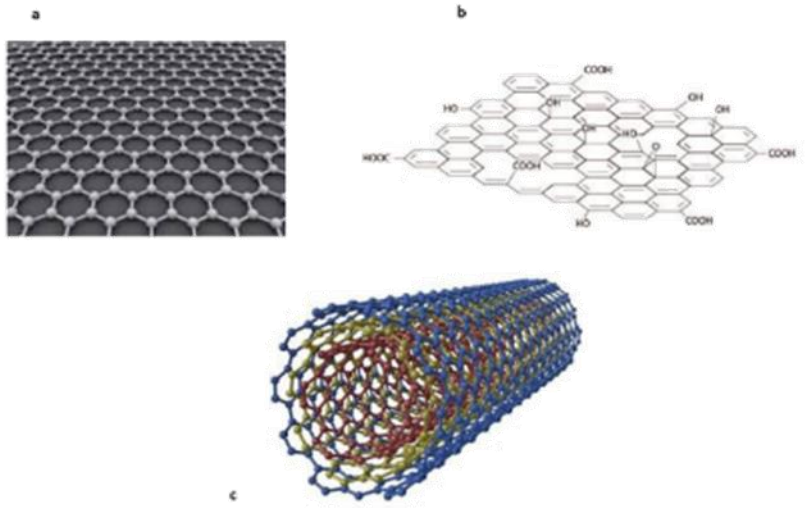

Figure 4.1: Carbon based Nano-materials (a- Graphene, b- graphene oxide, c- CNT)

4.1.2 Applications of Graphene

Since its isolation, graphene has rapidly transitioned from a scientific curiosity to a critical material with far-reaching technological implications. Its extraordinary physical and chemical properties—including exceptional electrical conductivity, mechanical strength, thermal stability, and large specific surface area—have laid the foundation for a broad spectrum of applications [13]. These attributes enable graphene to perform in ways that surpass conventional materials, making it an attractive candidate for next-generation technologies.

In electronics, graphene's high carrier mobility and atomic thinness have spurred research into faster, smaller, and more energy-efficient transistors, sensors, and flexible displays [14]. In particular, graphene-based field-effect transistors (GFETs) and transparent conductive films are being explored as alternatives to silicon and indium tin oxide (ITO), respectively.

Graphene also holds great promise in energy-related applications. Its high surface area and excellent electrical conductivity make it ideal for electrodes in supercapacitors and batteries, particularly lithium-ion and sodium-ion systems [15]. These devices can benefit from enhanced charge storage capabilities, faster charging times, and longer lifespans when graphene is used as a structural or conductive additive.

In the field of composite materials, graphene's mechanical robustness and light weight have led to its integration into polymers, metals, and ceramics to create materials with superior strength, thermal conductivity, and corrosion resistance [16]. Such graphene-enhanced composites are being developed for use in aerospace, automotive, and sports equipment industries.

Graphene's biocompatibility and functionalizability also position it as a transformative material in biomedical applications, including biosensors, drug delivery systems, tissue engineering scaffolds, and antibacterial coatings [17]. Its surface can be engineered to interact with biological molecules, enabling sensitive and selective detection or targeted therapeutic delivery.

Moreover, graphene is being utilized in environmental technologies, such as water purification membranes, pollutant adsorbents, and gas separation systems [18]. Its ultrathin, yet strong and chemically stable structure allows for efficient filtration and molecular sieving at a nanoscale level.

Despite these promising developments, many graphene-based technologies remain at the prototype or early commercialization stage. Challenges such as scalable production, consistent material quality, and integration with existing manufacturing processes continue to limit widespread adoption. However, ongoing research and industrial interest are rapidly addressing these barriers, bringing graphene-based solutions closer to market readiness.

4.1.3 Graphene Oxide (GO)

Graphene oxide (GO) is a single-atomic layered material derived from the oxidative treatment of graphite, consisting of a graphene-like carbon lattice decorated with oxygen-containing functional groups such as hydroxyl (–OH), epoxy (–O–), carbonyl (C=O), and carboxyl (–COOH) [19]. These groups disrupt the extended π-conjugation of graphene, transforming the sp^2-hybridized network into a mixed sp^2/sp^3 system. This modification imparts unique characteristics to GO, including hydrophilicity, high surface reactivity, and dispersibility in water and polar solvents—features that distinguish it from pristine graphene [20].

Originally described more than a century ago, GO has recently attracted renewed scientific attention due to its versatility, affordability, and its critical role as a scalable precursor to reduced graphene oxide (rGO) and graphene-like materials [21]. Its amphiphilic nature allows it to interact effectively with both hydrophilic and hydrophobic substances, while its high surface area and functional group density make it suitable for chemical functionalization and composite integration [22].

One of GO's most attractive features is its tunability. Depending on its oxidation level, GO can act as an insulator or a semiconductor. Through chemical, thermal, or electrochemical reduction, it can be partially restored to a more conductive state, producing rGO with properties that closely resemble those of graphene while retaining essential functional moieties [23]. This tunability has led to the use of GO in diverse fields, including electronics, sensors, energy storage, catalysis, and biomedicine.

Structurally, GO is highly non-stoichiometric, and its exact atomic arrangement remains a topic of ongoing research. The most widely accepted model describes it as a carbon sheet containing regions of unoxidized aromatic rings interspersed with sp^3-hybridized zones bearing oxygen functional groups [24]. This complex structure is responsible for its dual properties—chemical reactivity and mechanical stability.

GO is typically synthesized via the Hummers' method or its modifications, involving strong oxidants such as potassium permanganate ($KMnO_4$) and concentrated sulfuric acid

(H_2SO_4) to break down graphite into functionalized monolayers [25]. Recent developments have focused on optimizing this process to improve yield, reduce toxicity, and enable the use of sustainable carbon sources, including petroleum by-products and biomass [26].

Overall, GO represents a pivotal material in the advancement of graphene-based technologies. Its processability, scalability, and tuneable characteristics make it a strategic component in nanotechnology, materials science, and environmental engineering.

4.1.4 Applications of Graphene Oxide (GO)

Graphene oxide (GO) has emerged as a highly versatile nanomaterial with broad applicability across numerous scientific and industrial domains. Its unique combination of properties—including high surface area, hydrophilicity, mechanical strength, and tenable electronic characteristics—has positioned it as a leading material in various cutting-edge technologies. The presence of oxygen-containing functional groups not only enables strong interactions with other materials but also allows for facile chemical modification, making GO highly adaptable for multifunctional systems [27].

4.1.4.1 Environmental Remediation

One of the most prominent applications of GO lies in wastewater treatment and environmental remediation. Due to its porous structure and abundant functional groups, GO exhibits excellent adsorption capabilities for a wide range of pollutants, including heavy metals (e.g., Pb^{2+}, Cd^{2+}), dyes (e.g., methylene blue), phenols, and oils [28]. Its hydrophilic nature enhances its dispersion in aqueous solutions, which in turn improves pollutant contact and removal efficiency. In addition to adsorption, GO has been used as a support material for photocatalysts, where it facilitates the photodegradation of organic contaminants under visible light irradiation [29].

4.1.4.2 Membrane Filtration Technologies

GO has also been extensively studied in membrane-based separation processes, including ultrafiltration, nanofiltration, and reverse osmosis. When incorporated into polymeric or

ceramic membranes, GO improves selectivity, water permeability, and antifouling resistance [30]. The layered structure of GO allows for the formation of tunable interlayer channels, enabling selective separation based on molecular size or charge. These GO-based membranes are particularly effective in desalination, dye rejection, and gas separation applications.

4.1.4.3 Biomedical Applications

In biomedicine, GO's biocompatibility and ease of functionalization have led to its use in drug delivery, biosensors, tissue engineering, and antimicrobial coatings [31]. Its high surface area enables the adsorption or covalent attachment of therapeutic agents, while its oxygen functional groups allow for conjugation with targeting ligands or biomolecules. Additionally, GO has been employed in photothermal therapy for cancer treatment, where its ability to absorb near-infrared radiation is used to generate localized heat and destroy cancer cells [32].

4.1.4.4 Energy Storage and Conversion

GO and its reduced form (rGO) are widely explored for use in energy storage devices, such as supercapacitors and lithium-ion batteries. In supercapacitors, GO enhances electrode surface area and electrolyte accessibility, improving specific capacitance and cycle stability [33]. In batteries, GO-based composites are used as anodes or cathode supports, offering better charge-discharge rates, electrical conductivity, and mechanical stability. Moreover, GO's functional groups serve as anchoring sites for metal ions and conductive additives, which improve energy density and lifespan.

4.1.4.5 Sensors and Flexible Electronics

Thanks to its tunable electrical properties, GO is also valuable in chemical and biosensing platforms. Its surface can be engineered to detect specific molecules, ions, or biological markers with high sensitivity and selectivity [34]. Additionally, its thin, flexible structure makes it suitable for use in wearable electronics, smart packaging, and flexible circuit

boards. GO is also being investigated for neuromorphic applications, such as in synaptic transistors, where it functions as a gate dielectric due to its proton conductivity [35].

4.1.4.6 Composite Materials

Incorporating GO into polymeric, metallic, or ceramic matrices can significantly enhance the mechanical, thermal, and electrical properties of the resulting composites. GO-reinforced composites are used in aerospace, automotive, and construction industries due to their improved tensile strength, impact resistance, and thermal stability [36]. Furthermore, GO improves the interfacial bonding between different material phases, thereby enhancing load transfer and durability.

4.1.5 Reduced graphene oxide (rGO)

Reduced graphene oxide (rGO) is a chemically or thermally treated derivative of graphene oxide (GO) in which a significant portion of oxygen-containing functional groups has been removed, partially restoring the conjugated sp^2 carbon network characteristic of pristine graphene [37]. This reduction process converts GO—originally an insulating, hydrophilic material—into a more conductive, hydrophobic material with enhanced mechanical and electronic properties. While rGO does not completely regain all the properties of pristine graphene, it offers a balance between performance and processability that makes it highly attractive for various practical applications.

The synthesis of rGO is typically achieved through several methods, including chemical reduction (using agents such as hydrazine, ascorbic acid, or sodium borohydride), thermal annealing, or electrochemical reduction [38]. Each method influences the extent of oxygen removal, the restoration of the graphene lattice, and the defect density in the final material. Consequently, the physical, chemical, and electrical properties of rGO can be tuned depending on the reduction conditions, enabling its use in targeted applications.

Compared to GO, rGO exhibits significantly improved electrical conductivity, due to the partial recovery of the π-electron conjugation. However, some residual oxygen groups and structural defects typically remain, which can be beneficial for specific applications such

as electrochemical sensors, composite reinforcement, or catalysis, where surface functional groups aid in binding or reactivity [39].

rGO is widely considered a cost-effective and scalable alternative to pristine graphene, especially for industrial applications that do not require the perfection of defect-free graphene sheets. Moreover, the synthesis of rGO from GO produced using petroleum residues, biomass, or industrial by-products offers a sustainable route for converting carbon-rich waste into high-value functional nanomaterials [40].

Due to its unique balance of conductivity, surface chemistry, and processability, rGO has found extensive application in energy storage devices, electronic components, environmental remediation, and biomedical systems. As research advances, efforts continue to improve the reduction methods to achieve higher conductivity and lower defect density, bridging the performance gap between rGO and pristine graphene.

4.1.6 Applications of Reduced Graphene Oxide (rGO)

Reduced graphene oxide (rGO), as a partially restored form of graphene, retains many of the unique properties of pristine graphene—such as high surface area, mechanical strength, and electrical conductivity—while maintaining processability due to residual oxygen-containing functional groups. This hybrid nature makes rGO highly attractive for a wide range of practical applications across energy, environmental, electronic, and biomedical fields [41]. Unlike pristine graphene, which is often expensive and difficult to produce at scale, rGO offers a cost-effective and scalable alternative with tunable surface chemistry and performance characteristics.

4.1.6.1 Energy Storage Devices

One of the most significant applications of rGO lies in energy storage technologies, particularly supercapacitors and lithium-ion batteries (LIBs). rGO-based electrodes demonstrate high specific capacitance, fast charge-discharge cycles, and excellent cycling stability due to their large surface area and restored electrical pathways [42]. In supercapacitors, rGO is used either as a standalone electrode material or in composites with metal oxides or conducting polymers to enhance charge storage. In LIBs, rGO serves as both a conductive network and a buffering matrix, improving electron transport and accommodating volume changes during lithiation/delithiation [43].

4.1.6.2 Environmental Remediation

rGO also plays a vital role in water purification and pollutant removal. Its high surface area, residual functional groups, and π–π interactions enable it to adsorb a wide range of contaminants, including heavy metals, organic dyes, oils, and pharmaceutical residues [44]. rGO is used in both powdered form and as a composite in adsorbents, membranes, and photocatalytic systems. Moreover, rGO-supported nanocomposites enhance photocatalytic degradation of pollutants under visible light, offering promising solutions for sustainable water treatment technologies [45].

4.1.6.3 Flexible and Printed Electronics

Due to its electrical conductivity and mechanical flexibility, rGO has been widely studied for use in flexible electronics, including transparent conductive films, printed circuits, and wearable sensors. rGO-based inks can be processed via inkjet printing, spray coating, or screen printing onto various substrates, enabling scalable production of flexible and low-cost electronic devices [46]. In particular, rGO is employed in strain sensors, capacitive touch sensors, and thin-film transistors for next-generation smart materials and devices.

4.1.6.4 Biomedical Applications

rGO's biocompatibility and surface tunability enable its application in drug delivery, biosensing, tissue engineering, and photothermal therapy. It can be functionalized with biopolymers, targeting ligands, or therapeutic agents to facilitate controlled release and selective delivery [47]. In cancer therapy, rGO absorbs near-infrared radiation and converts it into heat, making it effective for non-invasive photothermal ablation of tumor cells. Additionally, rGO is used in biosensors for detecting glucose, DNA, and proteins due to its electrochemical sensitivity and high surface-to-volume ratio [48].

4.1.6.5 Catalysis and Electrocatalysis

rGO serves as an excellent catalyst support material in various heterogeneous and electrocatalytic reactions, including oxygen reduction reactions (ORR), hydrogen evolution reactions (HER), and pollutant degradation. Its partially restored conjugated system enables fast electron transport, while residual oxygen groups serve as anchoring sites for metal nanoparticles or active moieties, enhancing overall catalytic activity and stability [49].

4.1.6.6 Composite and Structural Materials

In polymer nanocomposites, rGO is used as a nanofiller to improve mechanical, thermal, and barrier properties of the host matrix. It enhances tensile strength, elasticity, and flame retardancy in plastics, rubbers, and coatings. These rGO-reinforced materials are being explored in automotive, aerospace, and construction industries due to their lightweight nature and durability [50].

Property	Synthetic Graphite	Graphene Oxide (GO)	Reduced Graphene Oxide (rGO)	Reference
Structure	Layered sp^2 carbon atoms	Disordered carbon sheets with oxygen-	Partially restored sp^2 network with defects	[51]

	with ordered stacking	containing functional groups		
Surface Functional Groups	Negligible	Rich in –OH, –COOH, epoxy, and carbonyl groups	Few residual oxygen groups depending on reduction method	[52]
Hydrophilicity	Hydrophobic	Highly hydrophilic	Moderately hydrophobic	[53]
Electrical Conductivity	High	Very low (insulating)	Moderate to high (depending on reduction quality)	[54]
Dispersibility in Water	Poor	Excellent	Moderate	[55]
Mechanical Properties	High strength and modulus	Weakened due to oxidation	Improved over GO, but less than pristine graphene	[56]
Thermal Stability	Excellent	Decomposes at ~200–250 °C	Higher than GO but less than graphite	[57]
Production Method	Graphitization of carbonaceous materials at high temperature	Oxidation of graphite (e.g., Hummers' method)	Chemical, thermal, or electrochemical reduction of GO	[58]
Typical Applications	Electrodes, lubricants, refractories	Water purification, sensors, drug delivery, membranes	Supercapacitors, batteries, electronics, nanocomposites	[59]

Cost and Scalability	Cost-effective and widely scalable	Moderate cost, scalable	Scalable, but cost depends on reduction route	[60]

Table 4.1: Comparison of Synthetic Graphite, Graphene Oxide (GO), and Reduced Graphene Oxide (rGO)

4.2 Materials & Methods

4.2.1 Synthesis of Green, calcined and graphitized carbon

The VGO was pyrolyzed at 500°C for 10 min under inert atmospheric conditions as per ASTM D4530 resulting in the formation of green carbon. The obtained green carbon samples were further heat treated in two steps, followed by heating at 900°C with heating rate of 10°C and 1350°C with rate of 5°C and held for 30 min and 5 hr respectively to produce calcined carbon. This was done to remove all volatile matters for further processing to get graphitized carbon. Graphitization was done at 2800°C with heating rate of 15°C and held for 2 hr.

4.2.2. Synthesis of Graphene oxide

VGO-derived synthetic graphite is used as a basis in a modified Hummers' method to create graphene oxide (GO) fig 4.2. In this procedure, a 1:25:3 ratio of potassium permanganate ($KMnO_4$) to 98% pure sulfuric acid (H_2SO_4) is used to oxidize graphite samples (Pinto et al, 2017). For four hours, the reaction is kept at 5 °C to regulate the oxidation process. Next, add 5 milliliters of hydrogen peroxide ($H2O_2$) and stir for 15 minutes. Next, add 10 milliliters of 30% concentrated hydrochloric acid (HCl). Before adding cold water to the mixture, the mixture is given 15 minutes to settle. Sulfuric acid helps the graphite layers intercalate, and $KMnO_4$ is added gradually in an ice-cold environment to stop uncontrollably occurring exothermic reactions. Following the gradual addition, the reaction mixture is heated to about 40 °C and agitated for a few hours in order to incorporate functional groups that contain oxygen and facilitate the oxidation of graphite into graphene oxide (Amemiya et al, 2003). After the oxidation is finished, the reaction is

quenched with water and any remaining permanganate is neutralized with hydrogen peroxide, which turns the byproducts of manganese dioxide into soluble manganese ions. The resultant GO is purified by repeatedly washing it in distilled water to get rid of extra metal ions and acids. Next, it is dried under vacuum to keep its structure rich in oxygen.

The purified GO was then vacuum-dried to maintain its oxygen-rich structure while preventing agglomeration. The successful oxidation of graphite into GO was confirmed through X-ray diffraction (XRD) and Fourier-transform infrared spectroscopy (FTIR).

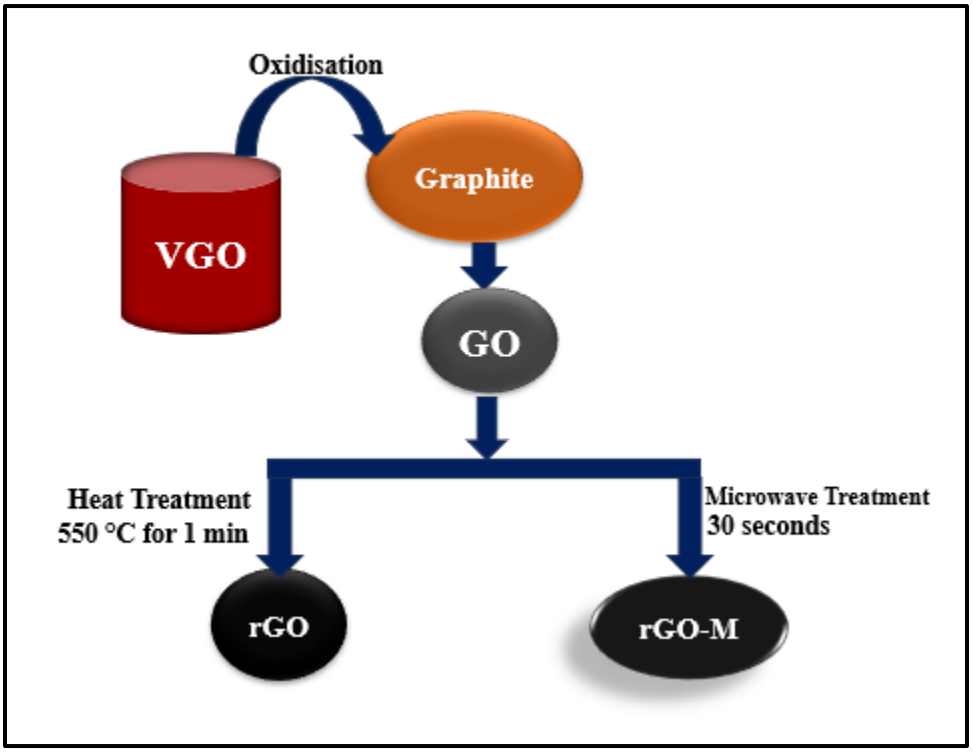

Figure 4.2: Schematic diagram showing the synthesis of rGO & rGO-M from VGO via microwave assisted method

4.2.3 Thermal Reduction of Graphene Oxide (RGO-Thermal)

Thermal reduction was employed as a key method to convert graphene oxide (GO) into thermally reduced graphene oxide (RGO-Thermal), aiming to restore the conjugated carbon network by eliminating oxygen-containing functional groups. The reduction process was carried out using a programmable tube furnace, where the as-prepared GO

samples were carefully placed in a quartz crucible and purged under a continuous flow of high-purity nitrogen (N_2) gas in order to maintain an inert atmosphere and prevent unwanted oxidation. The samples were then subjected to rapid thermal treatment at 550 °C for one minute, with the heating rate controlled to ensure uniform thermal exposure. This rapid high-temperature treatment triggered the exfoliation of stacked GO layers due to the sudden evolution of gaseous products, primarily carbon monoxide (CO) and carbon dioxide (CO_2), which originated from the decomposition of labile oxygen functionalities such as hydroxyl, epoxy, and carboxyl groups. The violent gas release facilitated the delamination of GO sheets, significantly reduced the interlayer spacing, and partially restored the sp^2-hybridized carbon domains. As a result, the RGO-Thermal samples exhibited a wrinkled and crumpled morphology, which is generally advantageous for enhancing surface area and improving electrical conductivity.

To monitor and confirm the structural transformation occurring during thermal reduction, X-ray diffraction (XRD) analysis was performed. The XRD patterns revealed the disappearance or shift of the characteristic diffraction peak associated with GO, indicating the removal of oxygen functionalities and the restoration of graphitic stacking. Furthermore, thermogravimetric analysis (TGA) was employed to systematically compare the thermal stability of pristine graphite, GO, and RGO-Thermal. The TGA profiles demonstrated distinct weight loss behaviors corresponding to the decomposition of oxygen-containing groups in GO and the enhanced stability achieved after reduction. The optimization of temperature and reduction time was found to be critical, as excessive thermal treatment could introduce structural defects, thereby compromising the electrical and mechanical properties of the material. Overall, the thermal reduction process provided an effective pathway for obtaining RGO with improved conductivity, tuneable surface chemistry, and enhanced structural integrity, suitable for subsequent characterization and application studies.

4.2.4 Microwave-Based Reduction of Graphene Oxide (RGO-Microwave or RGO-M)

Microwave-assisted reduction (RGO-M) was employed as a rapid, energy-efficient, and scalable alternative to conventional thermal reduction for the conversion of graphene oxide

(GO) into reduced graphene oxide. In this method, GO samples were exposed to microwave radiation with a fixed operating frequency of 2.45 GHz and variable power levels ranging from 200 W to 1000 W (Fig. 4.2). The samples were placed in a microwave-compatible quartz vessel to ensure uniform exposure and to prevent contamination during irradiation. The reduction process was completed within 30 seconds, highlighting the remarkable efficiency of microwave heating compared to conventional high-temperature reduction methods, which typically require extended durations and higher energy consumption (Bai et al., 2011).

The microwave irradiation interacts selectively with polar oxygen-containing functional groups, such as hydroxyl, epoxy, and carboxyl moieties, resulting in localized dielectric heating and bond cleavage. This localized heating leads to the decomposition of oxygen functionalities and the release of gaseous by-products, predominantly CO and CO_2, thereby promoting exfoliation and restoring the sp^2 carbon framework. Unlike thermal reduction, which often induces excessive structural damage due to uncontrolled gas evolution, the microwave-assisted process achieves a balance between effective deoxygenation and structural preservation. Consequently, RGO-M exhibits superior characteristics, including enhanced electrical conductivity, reduced defect density, and improved adsorption capacity. These properties render RGO-M particularly suitable for advanced environmental and energy-related applications, such as oil spill remediation, wastewater purification, supercapacitors, and battery electrodes.

To investigate the structural and morphological changes induced by microwave reduction, high-resolution transmission electron microscopy (HRTEM) was performed. HRTEM images revealed significant exfoliation of stacked graphene oxide sheets, with restored graphene layers displaying improved ordering and continuity of the conjugated carbon domains. The absence of large-scale sheet fragmentation confirmed that microwave treatment minimized structural damage while effectively reducing oxygen groups. Complementary spectroscopic and diffraction analyses further validated the successful conversion of GO to RGO-M, confirming the restoration of the graphitic structure and the enhancement of electrical conductivity.

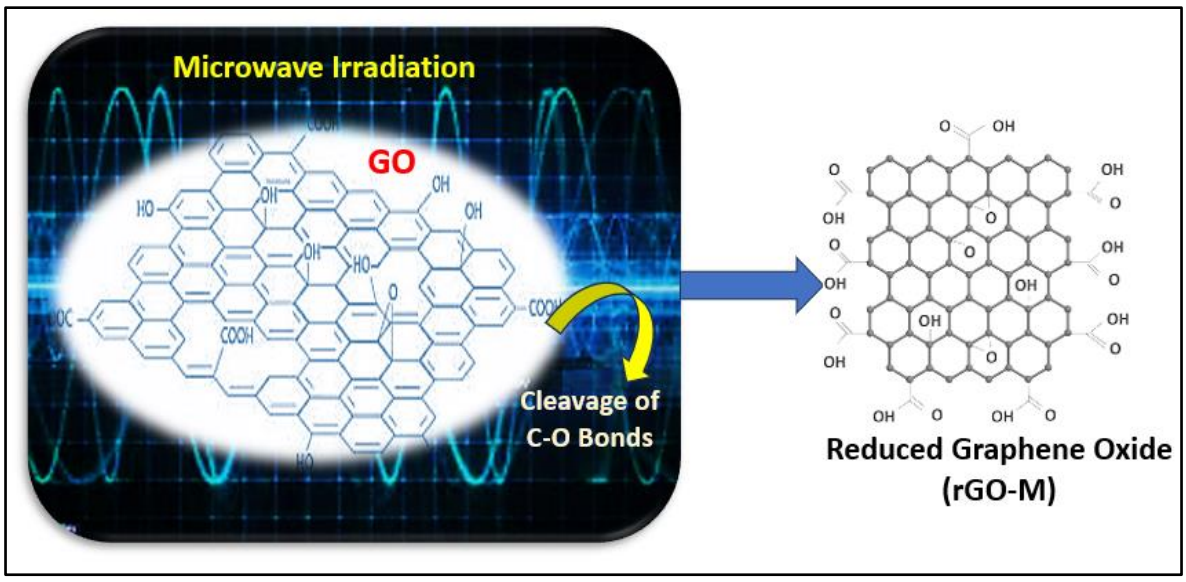

Figure 4.2: Schematic representation of the microwave-assisted reduction mechanism of graphene oxide (GO) to reduced graphe.3ne oxide modified (rGO-M).

4.2.5 ANALYSIS AND CHARACTERIZATION METHOD

4.2.5.1 Carbon Residue (ASTM D4530)

This method discussed in chapter 3 in section 3.2.1.

4.2.5.2 Elemental Analysis (CHNSO)

This method discussed in chapter 3 in section 3.2.2.

4.2.5.3 X-ray diffraction

This method discussed in chapter 3 in section 3.2.3.

4.2.5.4 Fourier Transform Infrared Spectroscopy

This method discussed in chapter 2 in section 2.2.8.

4.2.5.5 Thermogravimetric Analysis

This method discussed in chapter 3 in section 3.2.4.

4.2.5.6 Raman Spectroscopy

This method discussed in chapter 3 in section 3.2.5.

4.2.5.7 BET adsorption isotherm

The Brunauer–Emmett–Teller (BET) adsorption isotherm technique was employed to determine the specific surface area, pore volume, and pore size distribution of the synthesized graphene-based samples. BET analysis is widely recognized as a standard method for textural characterization of porous materials, catalysts, activated carbons, and nanostructured solids (Castro et al., 2021; Zhou et al., 2022). The principle of the method is based on the physical adsorption of nitrogen (N_2) molecules at liquid nitrogen temperature (77 K), where multilayer adsorption occurs on the solid surface.

The BET theory assumes multilayer adsorption and is expressed by the BET equation:

$$\frac{1}{V\left[\left(\frac{P_0}{P}\right)-1\right]} = \frac{C-1}{V_m C}\cdot\frac{P}{P_0} + \frac{1}{V_m C}$$

where:

- VVV = volume of gas adsorbed at pressure PPP,
- VmV_mVm = monolayer adsorbed gas quantity,
- P0P_0P0 = saturation pressure of the adsorbate gas (N_2),
- CCC = BET constant, related to the energy of adsorption.

From the BET plot (1V[(P0/P)−1] vs. P/P0)\left(\frac{1}{V[(P_0/P)-1]} \, \text{vs.} \, P/P_0\right)(V[(P0/P)−1]1vs.P/P0), the monolayer capacity (VmV, mVm) was obtained, which was then used to calculate the specific surface area of the material. The adsorption branch of the isotherm provided surface area data, while the desorption branch was used for pore volume and pore size distribution analysis.

The Barrett–Joyner–Halenda (BJH) method was further applied to the desorption isotherm to estimate mesopore size distribution, which is particularly important for evaluating materials designed for adsorption, catalysis, and energy storage applications. The

combination of BET and BJH analyses provided a comprehensive understanding of the pore structure and surface characteristics of the synthesized graphene-based materials.

In this study, nitrogen adsorption–desorption measurements were performed using a Quantachrome NOVAtouch 4LX surface area and porosity analyser. Prior to analysis, all samples were degassed under vacuum at 150 °C for 12 hours to remove adsorbed moisture and impurities, ensuring the accuracy of adsorption measurements. The instrument provided high-resolution isotherm data, from which the BET surface area, total pore volume, and pore size distribution were derived. The obtained results were used to evaluate the quality, porosity, and surface characteristics of the synthesized graphene-based materials, thereby establishing a correlation between synthesis methods and resulting structural properties.

4.2.8 Field Emission Scanning Electron Microscopy (FESEM)

Field Emission Scanning Electron Microscopy (FESEM) was employed to investigate the surface morphology and microstructural features of the synthesized samples with high spatial resolution. Unlike conventional SEM, which uses a thermionic electron source, FESEM utilizes a field emission gun (FEG) as the electron source, producing an electron beam of much smaller spot size and higher brightness. This results in enhanced resolution (typically below 2 nm) and improved imaging quality, making FESEM particularly suitable for analysing nanostructured materials such as reduced graphene oxide, porous carbons, and heterogeneous catalysts.

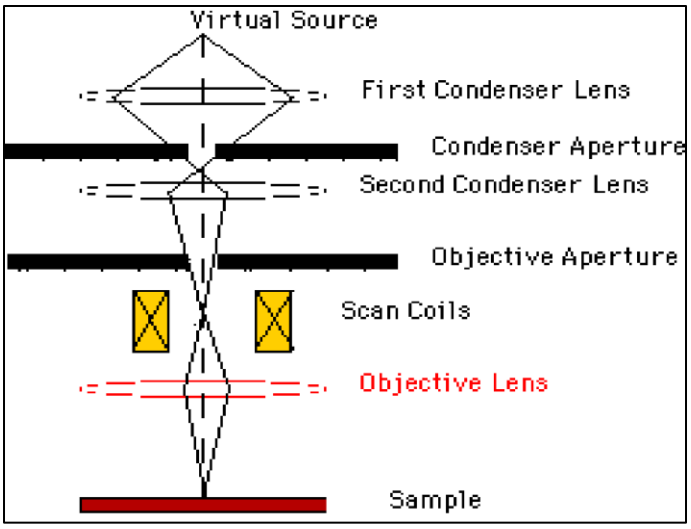

Figure 4.4 Schematic representation of scanning electron microscope

(Courtesy: http://www.unl.edu/CMRAcfem/em.htm)

In FESEM, the electron beam generated from the field emission source is focused through a system of electromagnetic lenses to form a finely converged probe. When the high-energy electron beam strikes the specimen surface, various signals are generated, including secondary electrons (SE), backscattered electrons (BSE), and characteristic X-rays. The SE signal, which is highly surface-sensitive, was primarily used for imaging surface morphology. These signals are collected by detectors and mapped into an image corresponding to the scanned region of the sample. The high beam current stability of FESEM also allows imaging at lower accelerating voltages, which is advantageous for delicate or non-conductive materials as it minimizes charging and beam damage.

For this study, FESEM analysis was carried out using a FEI Quanta 200 FEG Environmental Scanning Electron Microscope (ESEM, USA). Prior to imaging, the powdered samples were mounted onto aluminium stubs using carbon tape. To improve conductivity and reduce charging effects, selected samples were sputter-coated with a thin layer of gold (~5–10 nm). Imaging was performed under high-vacuum mode at accelerating voltages ranging from 5–20 kV, depending on the conductivity of the material. Multiple magnifications were recorded for each sample to analyse particle shape, sheet morphology, agglomeration behaviour, and pore structure.

FESEM provided detailed insights into the morphology of micro-, meso-, and composite catalysts. The images revealed surface roughness, wrinkled graphene sheets, and textural features that could be correlated with BET surface area and TEM/HRTEM analyses. This complementary morphological characterization was critical for establishing a structure–property relationship of the synthesized carbon-based materials.

4.2.9 High-Resolution Transmission Electron Microscopy (HRTEM)

Transmission Electron Microscopy (TEM) was utilized to investigate the morphology, crystallinity, and structural properties of the synthesized micro-, meso-, and composite catalysts at the nanoscale. Unlike Scanning Electron Microscopy (SEM), which provides surface morphology, TEM allows visualization of internal structures due to the transmission of a highly focused electron beam through ultrathin specimens. This enables the direct observation of particle size, pore distribution, and aggregation state, which are critical for understanding the structure–property relationship of nanomaterials.

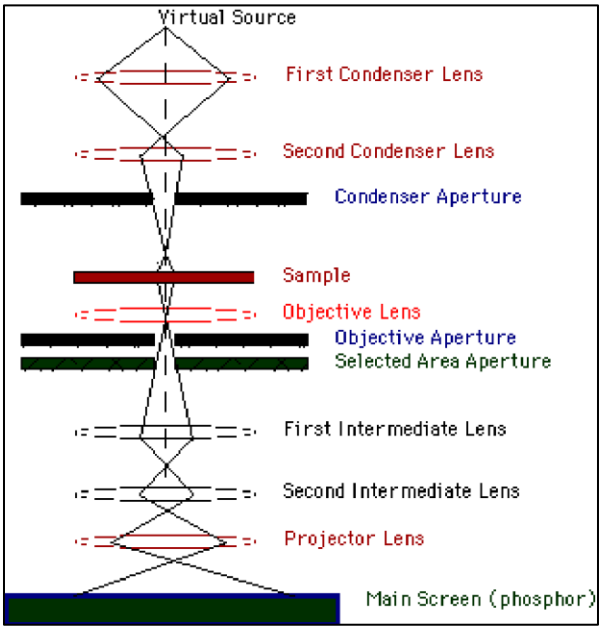

Figure 2.12

Figure 4.5. The schematic diagram of HRTEM

(Courtesy: http://www.unl.edu/CMRAcfem/em.htm)

In TEM, a monochromatic electron beam produced by the electron source is focused into a coherent stream by two condenser lenses. The condenser aperture restricts high-angle scattered and high-energy electrons, allowing only selectively aligned electrons to strike the specimen. As the electron beam interacts with the ultrathin sample, part of it is transmitted while other portions are scattered or absorbed. The transmitted electrons are collected and focused by the objective lens to form an image. Image contrast arises due to differences in electron transmission: dense regions scatter more electrons and appear darker, while less dense regions appear brighter. This results in the characteristic black-and-white images of TEM.

Further crystallographic information was obtained using Selected Area Electron Diffraction (SAED). By selecting a specific region of the sample using an aperture, electron diffraction patterns were recorded. The resulting concentric ring patterns corresponded to the crystal planes of the material, providing a fingerprint for identifying crystalline phases, interplanar spacings, and crystallinity levels of the porous materials under study.

In addition to conventional TEM, High-Resolution TEM (HRTEM) was employed to examine lattice fringes, interlayer spacing, and ordering within the graphene-based structures. HRTEM allows direct imaging of the atomic arrangement by phase-contrast imaging, enabling the visualization of graphitic layers and defects within reduced graphene oxide (RGO). This high-resolution technique was particularly useful for determining the degree of reduction in graphene oxide, the restoration of the sp^2-hybridized carbon network, and the presence of structural defects or disordered regions. The interlayer spacing values obtained from HRTEM images were compared with X-ray diffraction (XRD) data to validate structural restoration after reduction.

For this study, TEM and HRTEM analyses were carried out using a FEI TECNAI G^2 (T-30, S-Twin) transmission electron microscope, operated at an accelerating voltage of 300 kV. Sample preparation involved dispersing a small amount of the powdered catalyst in

ethanol, followed by ultrasonication to achieve a homogeneous suspension. A drop of the suspension was deposited onto a carbon-coated copper grid and allowed to dry at room temperature before examination. TEM micrographs were captured at varying magnifications to assess particle morphology and aggregation, while HRTEM images provided insights into lattice ordering and interlayer distances. SAED patterns were also recorded to confirm crystallinity and phase composition of the synthesized materials.

4.3 Results & Discussion

4.3.1 X-ray Diffraction Analysis of GO, rGO, and rGO-M

The XRD patterns shown in Figure 4.6(a–d) provide a comparative analysis of the crystalline structures of graphite, graphene oxide (GO), thermally reduced graphene oxide (rGO), and microwave-assisted reduced graphene oxide (rGO-M). As expected, the pristine graphite sample [Fig. 4.6(a)] exhibits a strong and sharp diffraction peak at approximately 26° (2θ), corresponding to the (002) reflection plane of the hexagonal graphitic structure. This sharp peak is characteristic of well-ordered graphitic layers with a high degree of crystallinity and minimal structural defects. Additional reflections observed around 44° and 77° correspond to the (101) and (110) planes, respectively, which further validate the presence of a highly ordered hexagonal crystal lattice. The narrow full width at half maximum (FWHM) of these peaks further confirms the crystalline nature of graphite.

In contrast, the XRD pattern of GO [Fig. 4.6(b)] demonstrates a significant change in structural features. The characteristic (002) reflection of graphite at ~26° disappears, and a new diffraction peak emerges at lower 2θ values (~11°), corresponding to a d-spacing of 7.6974 Å as shown in Table 4.2. This large interlayer spacing can be attributed to the successful oxidation of graphite, which introduces oxygen-containing functional groups (hydroxyl, epoxy, and carboxyl) between the carbon layers. These oxygen functionalities, along with intercalated water molecules, disrupt the π–π stacking of graphitic sheets and push the layers apart, resulting in a more disordered and amorphous structure. The broad

and less intense nature of the GO peak is indicative of reduced crystallinity, higher defect density, and the loss of long-range graphitic order due to extensive oxidation (Kaminski et al., 2024).

The XRD pattern of rGO [Fig. 4.6(c)] shows the partial restoration of the graphitic structure after thermal reduction. A broad diffraction peak appears around 24–26° (2θ), corresponding to a decreased d-spacing of 3.6091 Å compared to GO. This reduction in interlayer distance indicates the effective removal of a considerable fraction of oxygen functionalities and trapped water molecules during the reduction process. However, the broadness of the peak compared to pristine graphite suggests that complete restoration of long-range order has not been achieved. The persistence of structural defects, residual oxygen groups, and wrinkled morphology prevent the formation of perfectly ordered graphitic domains, resulting in moderate crystallinity (De Rezende Pinho et al., 2023).

Interestingly, the XRD profile of rGO-M [Fig. 4.6(d)] reveals sharper and more intense diffraction peaks compared to thermally reduced rGO, with the (002) reflection observed at ~26° corresponding to a d-spacing of 3.3960 Å, which is much closer to that of pristine graphite (3.3858 Å). This indicates that microwave-assisted reduction is more effective in removing oxygen functionalities and restoring the conjugated sp^2 carbon network. The sharpness and intensity of the peaks suggest a higher degree of crystallinity and better layer stacking, demonstrating that microwave treatment not only restores graphitization but also minimizes the introduction of structural defects. The rapid and selective heating effect of microwave irradiation likely facilitates localized bond cleavage and efficient oxygen removal, while preventing excessive damage to the graphene framework.

Overall, the progressive transformation observed in the XRD patterns highlights the structural evolution from highly ordered graphite → disordered GO → partially restored rGO → well-restored rGO-M. Graphite shows the highest crystallinity with minimal interlayer spacing, while GO demonstrates the most disordered and expanded structure due to oxidation. Upon reduction, both rGO and rGO-M exhibit decreasing d-spacing values, with rGO-M approaching that of pristine graphite, thus confirming its superior structural recovery. The d-spacing values listed in Table 5.1 reinforce these findings, where rGO-M

(3.3960 Å) demonstrates almost complete recovery of the graphitic arrangement compared to graphite (3.3858 Å), highlighting the efficiency of microwave-assisted reduction over conventional thermal methods.

Samples	d-spacing [Å]
Graphite	3.3858
Go	7.6974
rGO	3.6091
rGO-M	3.3960

Table 4.2: d-Spacing values for Graphite, GO, RGO, and RGO-M

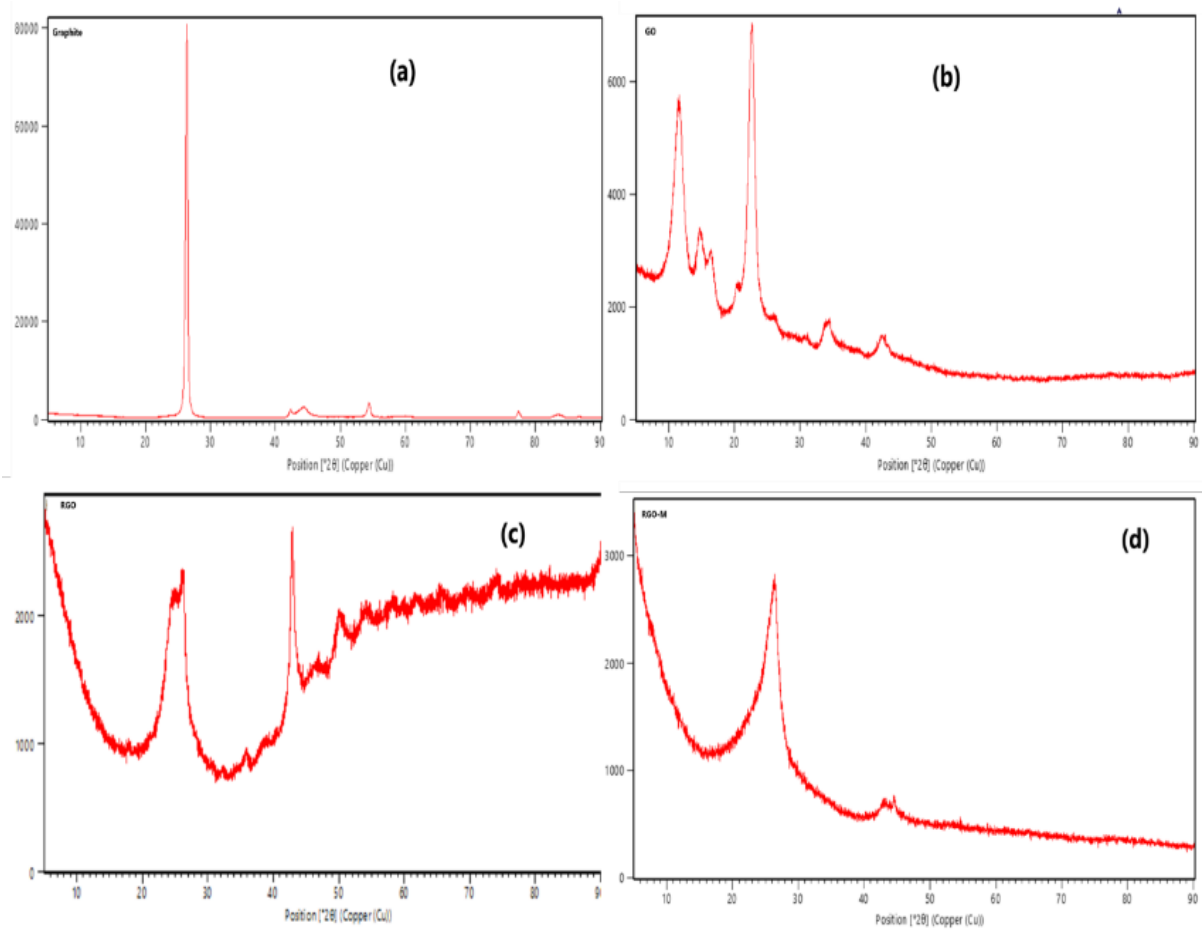

Figure 4.6: X-ray diffraction (XRD) patterns of samples (a) Graphite, (b) GO, (c) rGO and (d) rGO-M

4.3.2 Elemental Analysis (CHNSO) of GO, rGO, and rGO-M

The elemental composition of graphite, GO, rGO, and rGO-M, as summarized in Table 4.3, provides critical insights into the chemical transformations that occur during oxidation and subsequent reduction processes. These variations in carbon, hydrogen, nitrogen, sulphur, and oxygen contents directly reflect the degree of oxidation, the extent of reduction, and the possible incorporation of heteroatoms during synthesis and modification.

Pristine graphite, as expected, shows an almost pure carbon content of 99.99% with a negligible trace of nitrogen (0.01%), and no detectable hydrogen, sulphur, or oxygen. This confirms the crystalline nature of graphite, which is composed of stacked graphitic layers with extended sp^2 hybridized carbon networks and no oxygen functionalities (Amemiya et al., 2003; Titov et al., 2024). The absence of heteroatoms validates its chemically inert and highly ordered nature, serving as the baseline material for subsequent oxidation and reduction treatments.

In contrast, the elemental composition of GO indicates a substantial structural modification. The carbon content drops drastically to 47.04%, accompanied by a very high oxygen content of 46.30%. This significant increase in oxygen is consistent with the introduction of oxygen-containing functional groups such as hydroxyl, epoxy, carbonyl, and carboxyl groups during the Hummers oxidation process. The calculated C/O ratio of 1.02 further confirms the heavy oxidation of the graphene framework, highlighting a near one-to-one atomic ratio of carbon to oxygen. In addition to oxygen, GO also exhibits the presence of sulfur (2.57%), which is attributed to the use of sulfuric acid during the oxidation process, as well as nitrogen (0.25%) and hydrogen (3.84%), which suggest minor incorporation of functional groups and intercalated water molecules. The broad functionalization of GO explains its hydrophilic nature, higher defect density, and loss of electrical conductivity.

Upon thermal reduction, the chemical composition of rGO reveals a significant restoration of carbon content to 91.81%, accompanied by a drastic decrease in oxygen concentration

to 5.60%. This results in a markedly improved C/O ratio of 16.39, which demonstrates the efficient removal of oxygen functionalities. However, the values also reveal the persistence of some residual heteroatoms: nitrogen (0.94%) and sulfur (0.84%), which may originate from the reduction environment or incomplete removal of precursor impurities. The presence of low oxygen but measurable amounts of heteroatoms indicates that rGO possesses partially restored conductivity while retaining surface functionalities that can be advantageous for specific applications such as catalysis or adsorption.

Interestingly, rGO-M exhibits the most advanced reduction and structural restoration among the samples. The carbon content increases further to 96.18%, while oxygen concentration is minimized to just 0.31%, yielding an exceptionally high C/O ratio of 310.26. This clearly demonstrates the superior efficiency of microwave-assisted reduction in removing oxygen groups and restoring the conjugated sp^2 carbon framework. Compared to rGO, the microwave-assisted process appears to selectively eliminate oxygen with minimal disruption to the graphene lattice. The slightly higher hydrogen content (2.76%) and presence of sulfur (0.75%) in rGO-M suggest some degree of surface functionalization or residual groups, which may enhance its adsorption capacity and chemical reactivity. Notably, nitrogen is absent in rGO-M, indicating that no nitrogen incorporation occurred during the microwave treatment.

The progressive changes in the C/O ratio across the samples illustrate the transition from a highly oxidized state (GO, C/O ~1) to a partially reduced form (rGO, C/O ~16) and finally to a nearly pristine graphitic structure (rGO-M, C/O ~310). This trend highlights the superior performance of microwave-assisted reduction in achieving a material with minimal oxygen defects and enhanced structural recovery.

Sample	Carbon %	Hydrogen %	Nitrogen %	Sulphur %	Oxygen %	C/O Ratio
Graphite	99.99	0.00	0.01	0.00	0.00	-
GO	47.04	3.84	0.25	2.57	46.30	1.02
rGO	91.81	0.81	0.94	0.84	5.60	16.39
rGO-M	96.18	2.76	0.00	0.75	0.31	310.26

Table 4.3: Elemental composition of Graphite, GO, rGO, and rGO-M

4.3.3 Fourier Transform Infrared Spectroscopy of GO, rGO, and rGO-M

The FTIR spectra (Fig. 4.7) provide a detailed comparison of the functional group evolution across graphite, GO, rGO, and rGO-M, highlighting the chemical transformations during oxidation and reduction. As expected, graphite shows very few absorption peaks, reflecting its pristine state with a nearly pure sp^2 carbon framework and the absence of oxygen functionalities. This confirms the chemically inert and highly ordered structure of graphite, consistent with its XRD and elemental composition results.

Upon oxidation to form graphene oxide (GO), several new peaks emerge, clearly evidencing the introduction of oxygen-containing functional groups. A broad band around ~3400 cm^{-1} is attributed to the stretching vibrations of hydroxyl (–OH) groups, while a peak near ~2900 cm^{-1} corresponds to aliphatic C–H stretching. The strong absorption at ~1720 cm^{-1} indicates the presence of carbonyl (C=O) groups, typically associated with carboxylic acid and ketone functionalities. Furthermore, the distinct band at ~1100 cm^{-1} is assigned to epoxy (C–O–C) stretching vibrations. These spectral features confirm the extensive functionalization of GO with hydroxyl, carbonyl, epoxy, and ether groups. The incorporation of these oxygen functionalities is responsible for disrupting the conjugated sp^2 network, increasing hydrophilicity, and introducing structural disorder. Similar spectra of GO with intense oxygen-related peaks have been reported in earlier studies (Prado-Cerqueira et al., 2017; Poirier et al., 2016).

In the case of reduced graphene oxide (rGO), a significant decrease in the intensity of oxygen-related peaks is observed, reflecting the partial removal of oxygen functionalities upon reduction. The broad O–H band (~3400 cm^{-1}) is considerably diminished, suggesting substantial elimination of hydroxyl groups. The carbonyl peak at ~1720 cm^{-1} also weakens, although residual carbonyl and ether groups remain visible, consistent with incomplete reduction. The persistence of some oxygen functionalities indicates that conventional reduction is effective but not entirely capable of restoring the pristine graphitic structure. The reduction of hydroxyl groups is particularly prominent in rGO, which aligns with previous reports that thermal reduction favors the removal of more labile oxygen species (hydroxyl and epoxy) while leaving behind more stable carbonyl groups.

By contrast, microwave-assisted reduced graphene oxide (rGO-M) exhibits a more drastic reduction of oxygen functionalities. The O–H (~3400 cm^{-1}) and C=O (~1720 cm^{-1}) peaks are significantly suppressed, while the epoxy/ether C–O–C peak (~1100 cm^{-1}) is also strongly diminished. This indicates that microwave irradiation facilitates rapid and selective removal of oxygen groups, restoring a larger fraction of the sp^2 carbon framework in a short time. Interestingly, a comparison of rGO and rGO-M spectra reveals subtle differences in reduction pathways: while rGO appears more effective in eliminating hydroxyl groups, rGO-M demonstrates superior efficiency in reducing carbonyl functionalities. These variations suggest that the mechanisms of conventional thermal and microwave-assisted reductions differ, with microwave irradiation enabling localized heating and bond cleavage, thereby promoting a more uniform removal of stable oxygen moieties such as carbonyl groups.

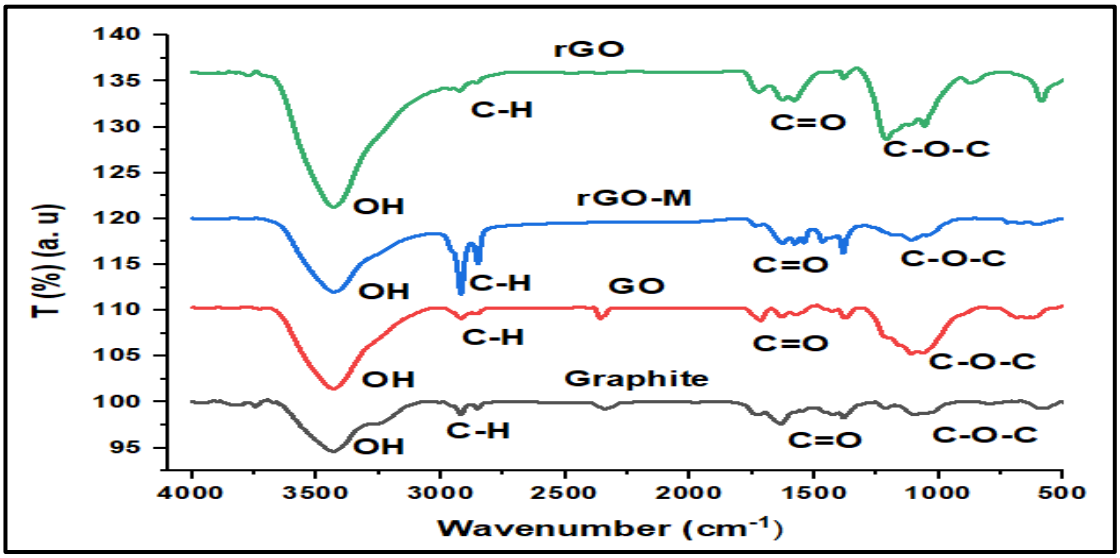

Figure 4.7: FTIR spectra of graphite, GO, rGO and rGO-M

4.3.4 Thermogravimetric Analysis of GO, rGO, and rGO-M

The TGA curves (Fig. 4.8) provide crucial insight into the thermal stability and decomposition behavior of graphite, GO, rGO, and rGO-M, thereby reflecting the extent of oxidation and reduction processes.

As expected, graphite exhibits excellent thermal stability, with negligible weight loss throughout the entire heating range up to 800 °C. This stability arises from its highly crystalline sp^2-hybridized carbon framework and the absence of labile functional groups, confirming its inert and ordered structure.

In contrast, GO displays significant weight loss in multiple stages, indicative of its unstable nature due to the abundance of oxygen-containing functional groups. The first minor weight loss below ~120 °C corresponds to the evaporation of physically adsorbed water molecules trapped within the interlayer spacing of GO. A sharp and substantial weight loss is observed between ~150 °C and 300 °C, which can be attributed to the decomposition of labile oxygen functionalities such as hydroxyl, epoxy, and carboxyl groups. Beyond 300 °C, GO continues to lose mass gradually up to 600–700 °C, associated with the decomposition of more stable oxygen species and the progressive breakdown of the carbon skeleton. This multistep degradation pattern underscores the poor thermal stability of GO, consistent with its high oxygen content as seen in elemental analysis (Table 5.2) and FTIR spectra (Fig. 4.8).

The rGO sample demonstrates a markedly different decomposition profile compared to GO, reflecting partial restoration of the sp^2 network. The initial weight loss below 120 °C is less pronounced, indicating reduced water absorption due to lower oxygen content. However, in the 200–800 °C range, rGO shows a noticeable weight loss, highlighting that it still retains a significant proportion of oxygen functionalities, particularly stable carbonyl and ether groups. This residual oxygen explains the broader, less intense XRD peaks (Fig. 4.8 c) and the incomplete suppression of FTIR signals. Thus, while rGO exhibits improved thermal resistance compared to GO, its reduction process does not completely eliminate oxygen functionalities, leaving behind structural defects that compromise its stability.

In contrast, rGO-M (microwave-reduced graphene oxide) exhibits the highest thermal stability among the reduced forms, with only minimal weight loss over the 200–800 °C temperature range. The smaller degree of mass loss reflects a more efficient removal of oxygen groups and a more complete restoration of the sp^2 carbon lattice. The microwave-assisted process facilitates localized, rapid heating that selectively targets oxygen

functionalities, particularly the more stable carbonyl species, resulting in a material with fewer defects and greater graphitization. This observation is strongly supported by the higher crystallinity in XRD (Fig. 4.8 d), the almost complete suppression of oxygen signals in FTIR (Fig. 4.8), and the very high C/O ratio in elemental analysis (Table 4.8). The improved stability of rGO-M aligns with previous reports (Hemmati-Sarapardeh et al., 2020; Hosseini et al., 2023) and confirms that microwave reduction is superior to conventional thermal reduction for producing structurally stable graphene-based materials.

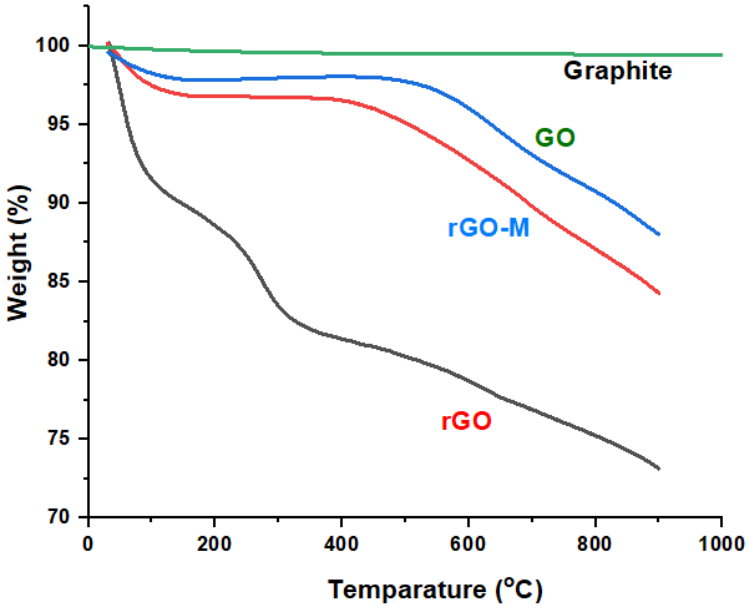

Figure 4.8: TGA curves showing thermal stability of graphite, GO, rGO and rGO-M.

4.3.5 Raman Spectroscopy of GO, and rGO-M.

The structural evolution of carbonaceous materials throughout the synthesis process was meticulously characterized using Raman spectroscopy, with key findings summarized in Fig 4.9 and Table 4.9. The Raman spectra served as a powerful tool to assess the degree of graphitization, defect density, and the restoration of the sp^2 carbon lattice following various reduction treatments.

The pristine graphite sample exhibited a classic Raman signature with two distinct, sharp peaks: the D band and the G band. The D band, located around 1350 cm^{-1}, is associated

with structural defects and disorder, while the G band, at approximately 1580 cm^{-1}, corresponds to the in-plane vibrational mode of sp^2-bonded carbon atoms. The crisp, well-defined nature of these bands, coupled with a remarkably low ID/IG ratio of 0.05, confirms the highly crystalline and low-defect nature of the starting material. In stark contrast, the Graphene Oxide (GO) spectrum showed a significant transformation. The D and G bands broadened substantially and were less pronounced. This widening is a direct consequence of the extensive oxidation process, which introduces numerous oxygen-containing functional groups (e.g., hydroxyl, epoxy, carboxyl) onto the basal plane of the graphene sheet. These functional groups disrupt the sp^2 network, leading to a high degree of structural disorder. The dramatic increase in the ID/IG ratio to 0.82 further corroborates the high concentration of defects, consistent with the structural instability described by Hendee et al. (1984).

Following reduction, both rGO (thermally reduced) and rGO-M (microwave-reduced) samples demonstrated a partial restoration of the graphitic structure. The Raman bands for both materials became noticeably sharper and more defined compared to GO. This sharpening indicates the successful removal of many of the oxygen functional groups and the reformation of the sp^2 carbon lattice. However, a closer examination reveals critical differences between the two reduction methods. The rGO-M sample exhibited a more pronounced and sharper peak profile, indicating a more effective and complete restoration of the sp^2 carbon network. This is further supported by the quantitative data in Table 5.3. While the ID/IG ratio for rGO increased to 1.01, the ratio for rGO-M showed an even greater increase, reaching 1.52. This seemingly counterintuitive rise in the ID/IG ratio is a key indicator of the formation of smaller, more numerous sp^2 domains within the rGO-M structure, as opposed to a simple restoration of the original graphite lattice.

The Raman spectroscopy results provide compelling evidence that microwave-assisted reduction is a superior method for producing high-quality reduced graphene oxide. The significant increase in the ID/IG ratio for rGO-M to 1.52, while initially appearing to suggest a higher defect density, actually signifies a successful restoration of the sp^2 carbon network by creating a large number of very small, high-quality graphitic domains. This phenomenon is characteristic of the rapid, localized heating provided by microwave

irradiation, which effectively "unzips" the basal planes and removes oxygen functional groups with minimal structural damage to the newly formed sp^2 domains. This interpretation is supported by FESEM analysis (as discussed in Section 4.2.8), which revealed a more uniform and exfoliated morphology for the rGO-M sample.

In contrast, the thermal reduction of rGO, while successful in removing some oxygen groups, appears to result in a less complete restoration of the graphitic structure, as evidenced by its lower ID/IG ratio (1.01). This suggests that the conventional heat treatment process is less efficient at creating the highly crystalline, yet numerous, graphitic domains observed in the microwave-reduced sample. The findings align with the literature (Rakhmatullin et al., 2022), which highlights the efficacy of microwave-assisted reduction in producing highly conductive and structurally refined graphene materials for various applications. The collective evidence from Raman spectroscopy and FESEM analysis unequivocally demonstrates that the microwave-assisted approach yields reduced graphene oxide with a higher degree of structural integrity and a closer resemblance to pristine graphite, making it a more desirable material for subsequent applications.

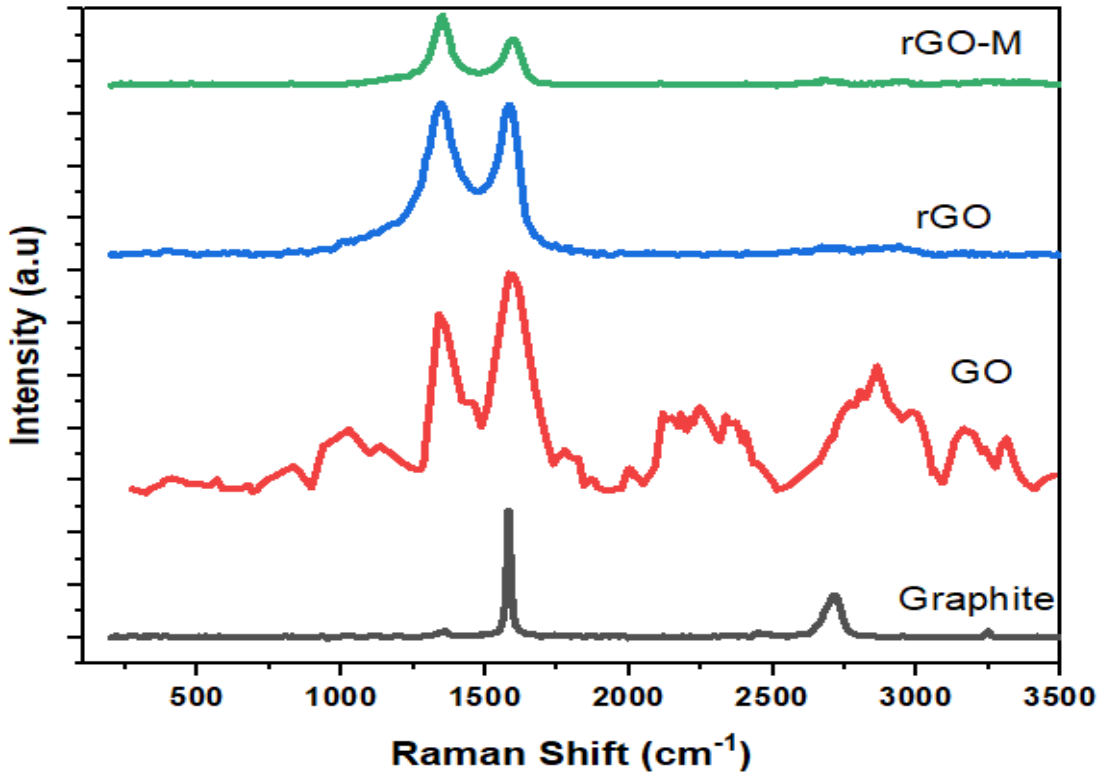

Figure 4.9: Raman spectra of graphite, GO, rGO, and rGO-M.

Sharper peaks in rGO-M indicate more effective reduction and restoration of the sp^2 carbon network compared to rGO and GO.

Sample Details	D- Band Position	D- Band Intensity	G- Band Position	G- Band Intensity	ID/IG
Graphite	1358.6	6.1	1580.8	121.4	0.05
GO	1337.9	177.9	1582.4	216.3	0.82
rGO	1345.9	145.0	1583.9	143.1	1.01
rGO-M	1350.6	65.9	1594.7	43.5	1.52

Table 4.4: Raman spectroscopy data of Graphite, GO, rGO, and rGO-M.

4.3.6 BET adsorption Isotherm of rGO and rGO-M.

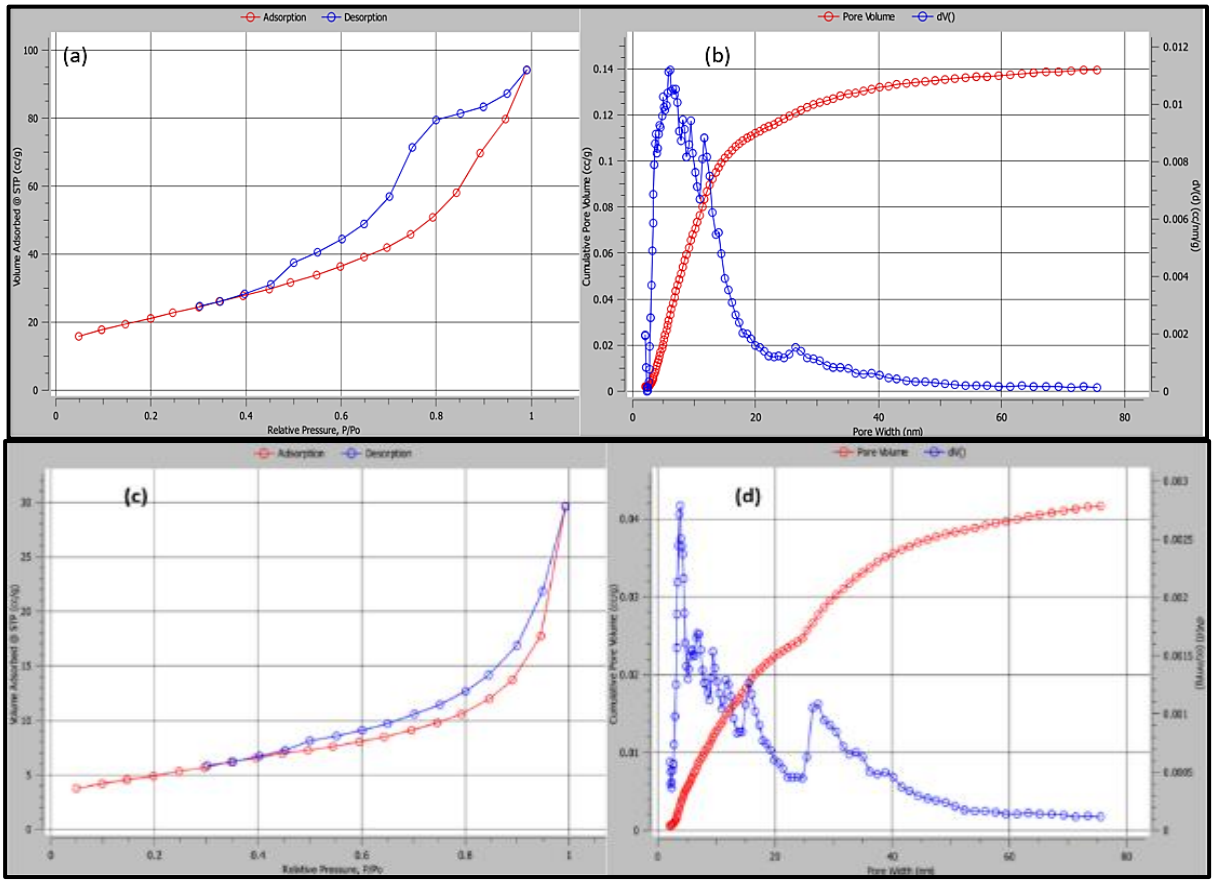

Figure 4.10: N_2 adsorption-desorption isotherms and pore size distribution of rGO and rGO-M.

The porous structure of rGO and rGO-M was systematically investigated through N_2 adsorption-desorption isotherms at 77 K. The resulting Brunauer-Emmett-Teller (BET) plots, as shown in Fig. 5.5, provide crucial insights into the surface area and pore size distribution of the two materials. Both rGO and rGO-M exhibit a Type IV isotherm with a distinct hysteresis loop at high relative pressures (P/P0>0.4), which is characteristic of mesoporous materials (Sharma et al., 2020; Wang et al., 2017). This indicates the presence of mesopores (2-50 nm) and macro pores (>50 nm), which arise from the disordered stacking of graphene sheets.

A key finding from this analysis is the significant difference in surface area and pore volume between the two materials. The rGO sample exhibited a surface area of 100 $m^2 g^{-1}$ with a micropore volume of 0.14 $cm^3 g^{-1}$. In contrast, the rGO-M sample had a much lower surface area of only 30 $m^2 g^{-1}$, accompanied by a lower micropore volume of 0.04 $cm^3 g^{-1}$. While a higher surface area is often correlated with better adsorption capacity, the pore size distribution profiles (Fig. 4.10b and Fig. 4.10d) reveal a more nuanced story. The rGO sample's high surface area is primarily attributed to a dense network of micropores (<2 nm). These ultra-small pores contribute significantly to the total surface area but are often not easily accessible to larger molecules or ions, limiting their effectiveness for certain applications like wastewater treatment.

Conversely, the rGO-M sample, despite its lower overall surface area, possesses a greater proportion of mesopores and macro pores. This is a direct result of the rapid and explosive exfoliation caused by microwave irradiation, which effectively separates the graphene sheets, creating a more open and interconnected porous structure. This structural development is highly beneficial for practical applications, as mesopores and macro pores offer multiple advantages. They facilitate rapid ion diffusion and mass transfer of target pollutants to the active adsorption sites, overcoming the diffusion limitations associated with micropores. This is particularly critical in applications such as wastewater treatment and oil spill clean-up, where the swift and efficient movement of contaminants within the porous network is essential for high performance.

Therefore, although the traditional metric of high surface area favours rGO, the pore size distribution analysis indicates that rGO-M is the more promising material for adsorption-based applications. The presence of a greater volume of larger pores ensures a more efficient and rapid adsorption process, as it provides clear pathways for molecules to access the interior surfaces. This finding is consistent with the FESEM analysis, which showed a less aggregated and more open structure for the microwave-reduced sample, further supporting the conclusion that microwave treatment yields a structurally superior material for these specific applications.

4.3.7 Field Emission Scanning Electron Microscopy of GO and rGO-M

The morphological evolution of the materials from pristine graphite to the final reduced graphene oxide products was meticulously examined using Field Emission Scanning Electron Microscopy (FESEM). The images, presented in Fig. 4.11, provide visual evidence of the structural changes induced by the oxidation and subsequent reduction processes.

Pristine graphite (Fig. 4.11a) exhibited a characteristic lamellar structure, with smooth, densely packed, and highly organized layers. This morphology is a direct result of the strong van der Waals forces holding the graphene sheets together in a highly ordered stacking. The absence of wrinkles or defects underscores the material's high crystallinity and structural integrity.

The transformation to graphene oxide (GO) (Fig. 4.11b) resulted in a dramatic change in morphology. The ordered lamellae were replaced by a collapsed, crumpled, and more amorphous sheet-like structure. This profound change is a direct consequence of the extensive oxidation process, which introduces a high concentration of oxygen-containing functional groups onto the basal planes and edges of the graphene sheets. These functional groups disrupt the π-electron system and weaken the inter-sheet interactions, leading to a significant increase in surface roughness and the formation of numerous wrinkles and folds, consistent with the findings of Adebiyi et al. (2014). This change in morphology is

critical as it drastically increases the material's surface area and provides new active sites for chemical reactions and interactions.

Subsequent reduction of GO to rGO (Fig. 4.11c) and rGO-M (Fig. 4.11d) led to a partial restoration of the layered structure. In both cases, the sheet-like morphology was largely preserved, with a noticeable decrease in the number of wrinkles and a partial re-stacking of the sheets. This is attributed to the successful removal of many of the oxygenated species, which allows the carbon sheets to regain some of their structural cohesiveness. However, a key distinction emerges when comparing the two reduction methods. The FESEM image of rGO-M shows a more exfoliated and porous structure compared to the more stacked and agglomerated rGO. This is a direct consequence of the rapid and volumetric heating mechanism of microwave irradiation, which creates steam and gas bubbles that explosively separate the graphene sheets, preventing restacking and promoting a more open and porous morphology.

The resulting morphology of rGO-M, characterized by this highly exfoliated and accessible structure, is of significant importance for environmental applications such as wastewater treatment and oil spill clean-up. This open, porous network provides a greater number of exposed active sites and facilitates faster mass transport of pollutants to the material's surface. As confirmed by our N_2 adsorption-desorption isotherms (Section 4.3.1), this morphology leads to a more advantageous pore size distribution, favouring mesopores and macro pores that are ideal for the rapid diffusion of molecules. The enhanced morphological and structural properties of rGO-M, therefore, play a critical role in its superior adsorption capabilities, as noted by Salehzadeh et al. (2022).

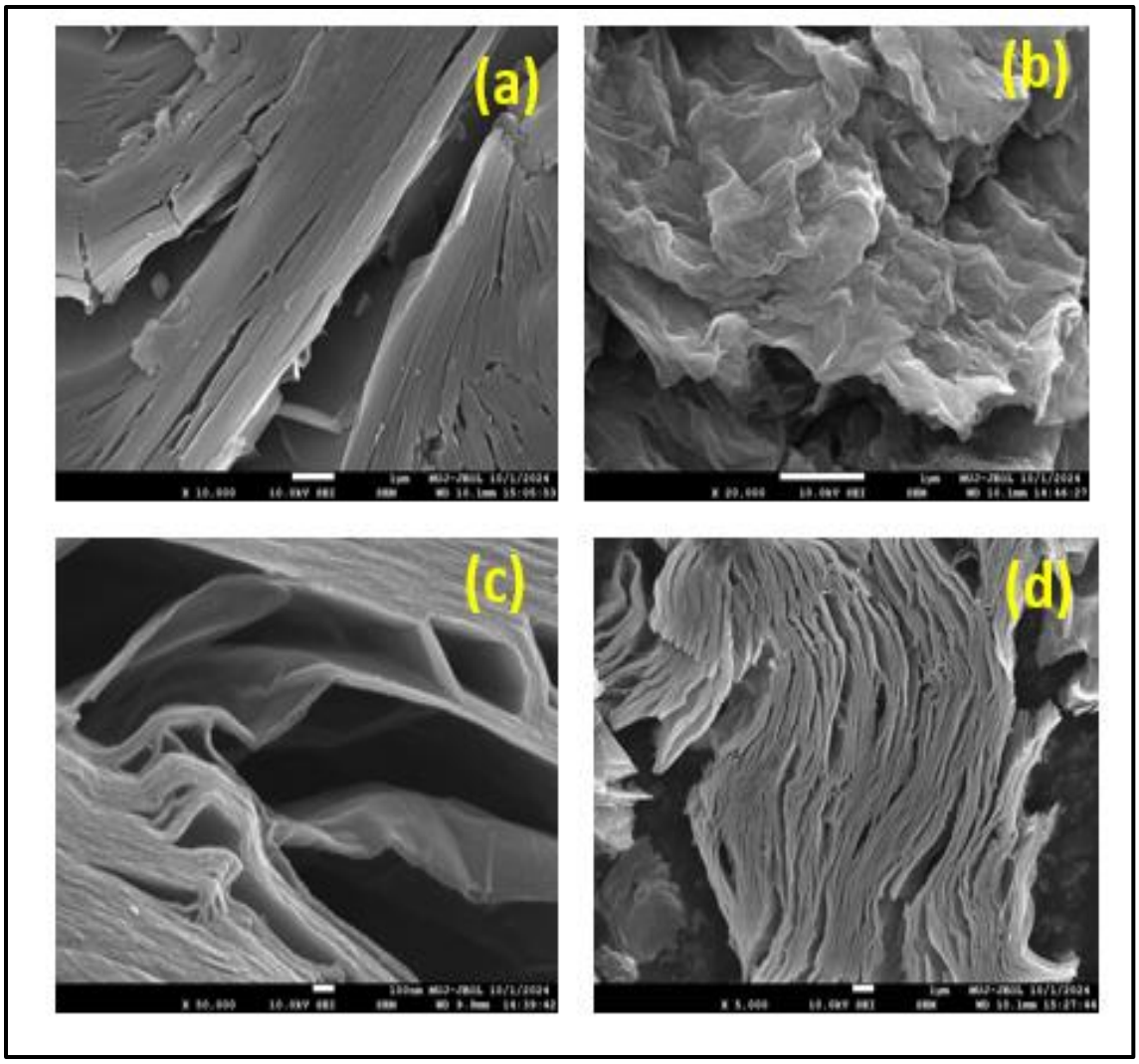

Figure 4.11: FESEM images showing the morphological evolution: (a) graphite; (b) GO; (c) rGO and (d) rGO-M

4.3.8 High-Resolution Transmission Electron Microscopy of GO and rGO-M

High-Resolution Transmission Electron Microscopy (HRTEM) analysis provided a detailed view of the structural changes at the atomic level, confirming the morphological and spectroscopic findings. The HRTEM images, presented in Fig. 4.12, reveal the crystalline evolution of graphitic carbon through oxidation and subsequent reduction processes.

Pristine graphitic carbon (Fig. 4.12a) showed a highly ordered and crystalline structure with well-aligned carbon layers, as evidenced by clear lattice fringes. This indicates a high degree of graphitization and a very low concentration of structural defects.

In contrast, the structure of graphene oxide (GO) (Fig. 4.12b) was severely disrupted. The ordered layers seen in graphite were replaced by a disorderly and loosely packed morphology. This disruption is a direct result of the oxidation process, which introduces oxygen-containing functional groups (e.g., carboxyl, hydroxyl, epoxide) between the layers. This process exfoliates the sheets and significantly increases the interlayer spacing, enhancing the material's chemical reactivity but destroying its long-range order. This observation is consistent with the findings of Canan et al. (2022) and Gao et al. (2024).

The thermally reduced graphene oxide (rGO) (Fig. 4.12c) showed a partial restoration of the graphitic layers. While some re-stacking occurred, the structure retained a significant amount of disorder, with numerous folds and wrinkles. This indicates that while thermal reduction removes many oxygen functionalities, it is less effective at fully reorganizing the sp^2 carbon network. The persistent disorder can negatively impact the material's electrical conductivity.

Conversely, the microwave-reduced graphene oxide (rGO-M) (Fig. 4.12d) exhibited a more significant restoration of the sp^2-hybridized carbon network. The HRTEM image shows more organized graphene layers and a clearer reorganization of the structure compared to rGO. The rapid, localized heating of the microwave-assisted process effectively eliminates a large number of oxygen functional groups and minimizes the re-stacking of sheets. While some residual disorder remains, which is characteristic of materials produced by microwave synthesis, the overall structural integrity is greatly improved. This superior structural recovery directly translates to enhanced electrical conductivity and a larger accessible surface area, making rGO-M highly suitable for a range of environmental applications, as noted by Gao et al. (2024).

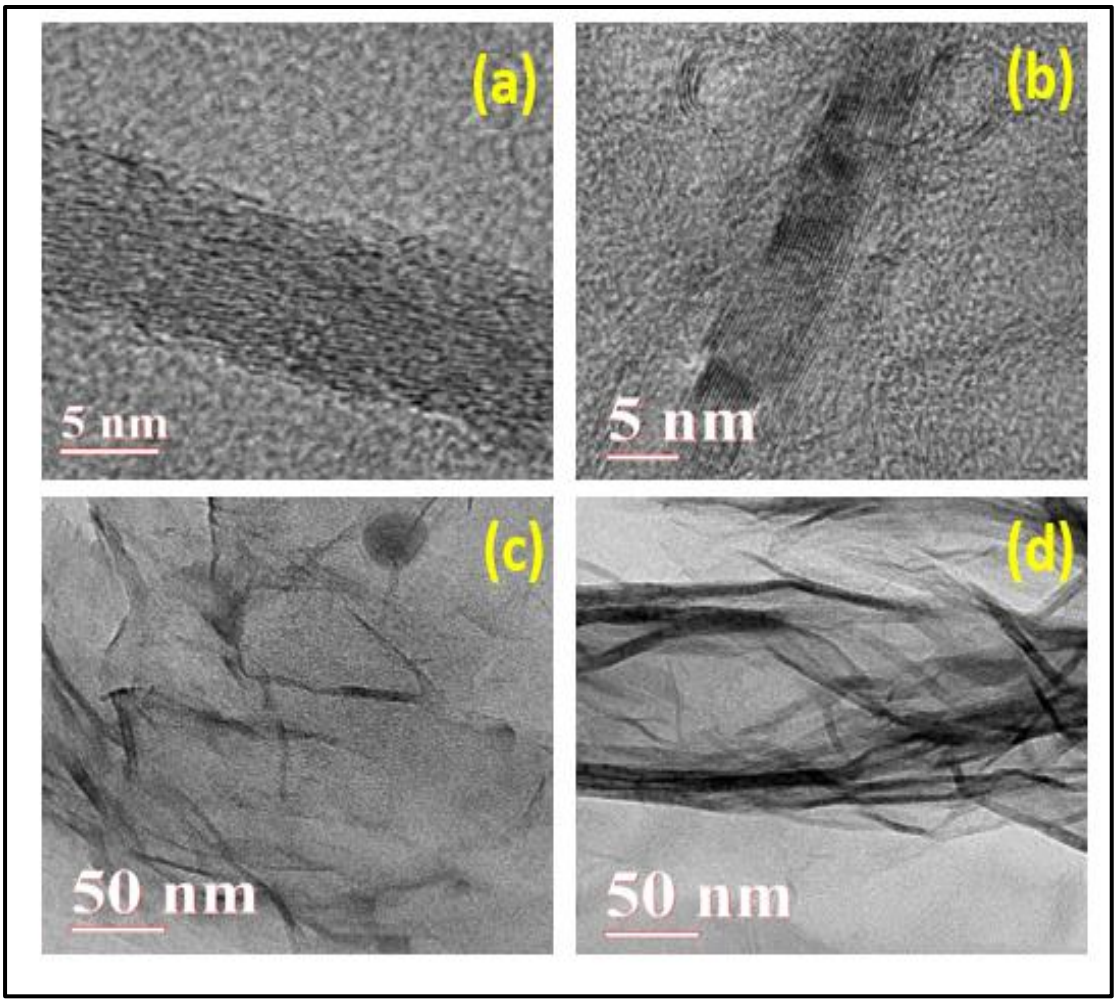

Figure 4.12: HRTEM of (a) graphitic carbon, (b) GO, (c) rGO and (d) rGO-M.

4.4 Conclusion

The comprehensive characterization of graphite, graphene oxide (GO), thermally reduced graphene oxide (rGO), and microwave-assisted reduced graphene oxide (rGO-M) using a suite of analytical techniques—including XRD, elemental analysis, FTIR, TGA, Raman spectroscopy, FESEM, and HRTEM—unequivocally demonstrates that microwave-assisted reduction is a superior method for producing high-quality graphene-based materials.

Structural Integrity: The XRD and HRTEM analyses showed a clear progression of structural changes. Graphite's highly crystalline, ordered structure was completely disrupted by oxidation, as evidenced by GO's broad XRD peak and expanded interlayer spacing. While thermal reduction (rGO) only partially restored this order, microwave reduction (rGO-M) resulted in a significantly more complete structural recovery, with a d-spacing value (3.3960 Å) remarkably close to that of pristine graphite (3.3858 Å).

Chemical Composition: Elemental analysis and FTIR confirmed the chemical transformations. The high oxygen content in GO was drastically reduced in both rGO and rGO-M. However, rGO-M demonstrated superior efficiency, achieving an exceptionally high C/O ratio of 310.26, indicating the almost complete removal of oxygen functionalities and a high degree of sp^2 carbon network restoration.

Thermal Stability: TGA results reinforced these findings, showing that rGO-M has the highest thermal stability among the reduced forms, reflecting its low oxygen content and superior structural integrity. This is in stark contrast to rGO, which showed greater residual mass loss due to incomplete reduction.

Morphology and Pore Structure: The FESEM and BET analyses provided crucial insights into the materials' morphology and porosity. While rGO had a higher surface area driven by inaccessible micropores, rGO-M exhibited a more exfoliated and porous structure with a higher proportion of accessible mesopores and macropores. This structural advantage, created by the explosive exfoliation during microwave treatment, is critical for applications requiring rapid diffusion and mass transfer, such as wastewater treatment.

Raman Spectroscopy: The Raman spectroscopy results provided final confirmation of the structural quality. The significant increase in the ID/IG ratio for rGO-M (1.52) compared to rGO (1.01) is a key indicator of the formation of numerous, high-quality graphitic domains. This phenomenon is a direct result of the microwave-assisted reduction process, which creates a more effective and refined sp^2 carbon network, even with residual disorder.

In conclusion, the collective evidence from all characterization techniques demonstrates that microwave-assisted reduction is more effective than conventional thermal reduction.

It produces a reduced graphene oxide material (rGO-M) that not only has higher structural integrity and a more complete restoration of the graphitic sp^2 network but also possesses a more favorable porous morphology for a wide range of environmental applications. The superior properties of rGO-M, including its high crystallinity, excellent thermal stability, and advantageous pore structure, position it as a highly promising and functional material for future research and industrial use.

References

1. Smith, D., & Johnson, M. (2018). Thermal stability and carbon residue of petroleum feedstocks: Analytical approaches and industrial implications. *Fuel, 222*, 312–320. https://doi.org/10.1016/j.fuel.2018.02.043
2. ASTM International. (2020). *ASTM D4530-20 Standard Test Method for Conradson Carbon Residue of Petroleum Products*. ASTM International.
3. Lee, S. Y., Kim, J. H., & Park, C. H. (2019). Characterization and upgrading of vacuum gas oil for enhanced catalytic cracking. *Journal of Petroleum Science and Engineering, 176*, 678–686. https://doi.org/10.1016/j.petrol.2019.02.024
4. Chen, L., Zhao, H., Li, J., & Xu, Y. (2021). Influence of heavy aromatic compounds on coke formation in vacuum gas oil catalytic cracking. *Fuel Processing Technology, 212*, 106620. https://doi.org/10.1016/j.fuproc.2020.106620
5. Martinez, A., & Singh, P. (2017). Coke formation mechanisms during catalytic cracking of vacuum gas oil: A review. *Energy & Fuels, 31*(8), 8393–8405. https://doi.org/10.1021/acs.energyfuels.7b01335
6. Gupta, R., & Roy, S. (2020). Catalyst deactivation i n fluid catalytic cracking: Role of carbon residue. *Catalysis Reviews, 62*(4), 478–507. https://doi.org/10.1080/01614940.2020.1785643
7. Wang, Y., & Zhao, Q. (2022). Impact of feedstock carbon residue on FCC unit performance and coke yield. *Chemical Engineering Journal, 429*, 132237. https://doi.org/10.1016/j.cej.2021.132237
8. Novoselov, K. S., Geim, A. K., Morozov, S. V., Jiang, D., Zhang, Y., Dubonos, S. V., ... & Firsov, A. A. (2004). Electric field effect in atomically thin carbon films. *Science, 306*(5696), 666–669. https://doi.org/10.1126/science.1102896
9. Geim, A. K., & Novoselov, K. S. (2007). The rise of graphene. *Nature Materials, 6*(3), 183–191. https://doi.org/10.1038/nmat1849
10. Allen, M. J., Tung, V. C., & Kaner, R. B. (2009). Honeycomb carbon: A review of graphene. *Chemical Reviews, 110*(1), 132–145. https://doi.org/10.1021/cr900070d

11. Zhu, Y., Murali, S., Cai, W., Li, X., Suk, J. W., Potts, J. R., & Ruoff, R. S. (2010). Graphene and graphene oxide: synthesis, properties, and applications. *Advanced Materials, 22*(35), 3906–3924. https://doi.org/10.1002/adma.201001068
12. Hernandez, Y., Nicolosi, V., Lotya, M., Blighe, F. M., Sun, Z., De, S., ... & Coleman, J. N. (2008). High-yield production of graphene by liquid-phase exfoliation of graphite. *Nature Nanotechnology, 3*(9), 563–568. https://doi.org/10.1038/nnano.2008.215
13. Bonaccorso, F., Lombardo, A., Hasan, T., Sun, Z., Colombo, L., & Ferrari, A. C. (2012). Production and processing of graphene and 2d crystals. Materials Today, 15(12), 564–589. https://doi.org/10.1016/S1369-7021(13)70014-2
14. Schwierz, F. (2010). Graphene transistors. Nature Nanotechnology, 5(7), 487–496. https://doi.org/10.1038/nnano.2010.89
15. Stoller, M. D., Park, S., Zhu, Y., An, J., & Ruoff, R. S. (2008). Graphene-based ultracapacitors. Nano Letters, 8(10), 3498–3502. https://doi.org/10.1021/nl802558y
16. Kim, H., Abdala, A. A., & Macosko, C. W. (2010). Graphene/polymer nanocomposites. Macromolecules, 43(16), 6515–6530. https://doi.org/10.1021/ma100572e
17. Liu, Y., Dong, X., & Chen, P. (2012). Biological and chemical sensors based on graphene materials. Chemical Society Reviews, 41(6), 2283–2307. https://doi.org/10.1039/C1CS15270J
18. Nair, R. R., Wu, H. A., Jayaram, P. N., Grigorieva, I. V., & Geim, A. K. (2012). Unimpeded permeation of water through helium-leak–tight graphene-based membranes. Science, 335(6067), 442–444. https://doi.org/10.1126/science.1211694
19. Lerf, A., He, H., Forster, M., & Klinowski, J. (1998). Structure of graphite oxide revisited. *The Journal of Physical Chemistry B, 102*(23), 4477–4482. https://doi.org/10.1021/jp9731821
20. Dreyer, D. R., Park, S., Bielawski, C. W., & Ruoff, R. S. (2010). The chemistry of graphene oxide. *Chemical Society Reviews, 39*(1), 228–240. https://doi.org/10.1039/B917103G

21. Loh, K. P., Bao, Q., Eda, G., & Chhowalla, M. (2010). Graphene oxide as a chemically tunable platform for optical applications. *Nature Chemistry, 2*(12), 1015–1024. https://doi.org/10.1038/nchem.907
22. Jayachandiran, J., Haribabu, M., & Arunachalam, P. (2018). Graphene oxide and its composites for the removal of pollutants from wastewater: A review. *Environmental Nanotechnology, Monitoring & Management, 9*, 96–104. https://doi.org/10.1016/j.enmm.2017.12.004
23. Pei, S., & Cheng, H. M. (2012). The reduction of graphene oxide. *Carbon, 50*(9), 3210–3228. https://doi.org/10.1016/j.carbon.2011.11.010
24. He, H., Klinowski, J., Forster, M., & Lerf, A. (1998). A new structural model for graphite oxide. *Chemical Physics Letters, 287*(1–2), 53–56. https://doi.org/10.1016/S0009-2614(98)00135-5
25. Hummers, W. S., & Offeman, R. E. (1958). Preparation of graphitic oxide. *Journal of the American Chemical Society, 80*(6), 1339. https://doi.org/10.1021/ja01539a017
26. Sadiq, M. M., Khan, T. A., & Ahmed, S. (2016). Controlled synthesis of graphene-based nanomaterials from petroleum residues for sustainable development. *Journal of Environmental Chemical Engineering, 4*(4), 4658–4666. https://doi.org/10.1016/j.jece.2016.08.012
27. Pei, S., & Cheng, H. M. (2012). The reduction of graphene oxide. *Carbon, 50*(9), 3210–3228. https://doi.org/10.1016/j.carbon.2011.11.010
28. Jayachandiran, J., Haribabu, M., & Arunachalam, P. (2018). Graphene oxide and its composites for the removal of pollutants from wastewater: A review. *Environmental Nanotechnology, Monitoring & Management, 9*, 96–104. https://doi.org/10.1016/j.enmm.2017.12.004
29. Zhang, H., Lv, X., Li, Y., Wang, Y., & Li, J. (2010). P25–graphene composite as a high performance photocatalyst. *ACS Nano, 4*(1), 380–386. https://doi.org/10.1021/nn901221k
30. Perreault, F., Tousley, M. E., & Elimelech, M. (2014). Thin-film composite polyamide membranes functionalized with biocidal graphene oxide nanosheets.

Environmental Science & Technology Letters, 1(1), 71–76. https://doi.org/10.1021/ez4001166

31. Yang, K., Feng, L., Shi, X., & Liu, Z. (2013). Nano-graphene in biomedicine: Theranostic applications. *Chemical Society Reviews, 42*(2), 530–547. https://doi.org/10.1039/C2CS35342C
32. Liu, Z., Robinson, J. T., Sun, X., & Dai, H. (2008). PEGylated nanographene oxide for delivery of water-insoluble cancer drugs. *Journal of the American Chemical Society, 130*(33), 10876–10877. https://doi.org/10.1021/ja803688x
33. Stoller, M. D., Park, S., Zhu, Y., An, J., & Ruoff, R. S. (2008). Graphene-based ultracapacitors. *Nano Letters, 8*(10), 3498–3502. https://doi.org/10.1021/nl802558y
34. Pumera, M. (2011). Graphene-based nanomaterials for electrochemical energy and biosensing applications. *Materials Today, 14*(7–8), 308–315. https://doi.org/10.1016/S1369-7021(11)70160-2
35. Wang, M., Liang, S., Wang, W., et al. (2020). Proton-conducting graphene oxide for neuromorphic electronics. *Advanced Functional Materials, 30*(27), 2002761. https://doi.org/10.1002/adfm.202002761
36. Kim, H., Abdala, A. A., & Macosko, C. W. (2010). Graphene/polymer nanocomposites. *Macromolecules, 43*(16), 6515–6530. https://doi.org/10.1021/ma100572e
37. Eda, G., & Chhowalla, M. (2010). Chemically derived graphene oxide: towards large-area thin-film electronics and optoelectronics. *Advanced Materials, 22*(22), 2392–2415. https://doi.org/10.1002/adma.200903689
38. Pei, S., & Cheng, H. M. (2012). The reduction of graphene oxide. *Carbon, 50*(9), 3210–3228. https://doi.org/10.1016/j.carbon.2011.11.010
39. Wang, Y., Shi, Z., Huang, Y., Ma, Y., Wang, C., & Chen, Y. (2009). Supercapacitor devices based on graphene materials. *The Journal of Physical Chemistry C, 113*(30), 13103–13107. https://doi.org/10.1021/jp902214f
40. Sadiq, M. M., Khan, T. A., & Ahmed, S. (2016). Controlled synthesis of graphene-based nanomaterials from petroleum residues for sustainable development. *Journal*

of Environmental Chemical Engineering, 4(4), 4658–4666. https://doi.org/10.1016/j.jece.2016.08.012

41. Eda, G., Fanchini, G., & Chhowalla, M. (2008). Large-area ultrathin films of reduced graphene oxide as a transparent and flexible electronic material. *Nature Nanotechnology, 3*(5), 270–274. https://doi.org/10.1038/nnano.2008.83
42. Stoller, M. D., Park, S., Zhu, Y., An, J., & Ruoff, R. S. (2008). Graphene-based ultracapacitors. *Nano Letters, 8*(10), 3498–3502. https://doi.org/10.1021/nl802558y
43. Zhou, G., Wang, D. W., Yin, L. C., et al. (2012). Oxygen bridges between reduced graphene oxide and SnO2 for lithium-ion battery anodes. *Advanced Materials, 24*(42), 625–629. https://doi.org/10.1002/adma.201202906
44. Zhang, N., Qiu, H., Si, Y., et al. (2019). Efficient removal of antibiotics from water using reduced graphene oxide-based magnetic nanocomposites. *Chemical Engineering Journal, 358*, 1153–1163. https://doi.org/10.1016/j.cej.2018.10.061
45. Yu, H., Zhang, B., & Bulin, C. (2013). Graphene-based photocatalytic composites for pollutant degradation. *Journal of Materials Chemistry A, 1*(12), 3695–3703. https://doi.org/10.1039/c3ta00056h
46. Torrisi, F., Hasan, T., Wu, W., et al. (2012). Inkjet-printed graphene electronics. *ACS Nano, 6*(4), 2992–3006. https://doi.org/10.1021/nn2044609
47. Yang, X., Zhang, X., Liu, Z., Ma, Y., Huang, Y., & Chen, Y. (2008). High-efficiency loading and controlled release of doxorubicin hydrochloride on graphene oxide. *Journal of Physical Chemistry C, 112*(45), 17554–17558. https://doi.org/10.1021/jp806751k
48. Mao, S., Pu, H., & Chen, J. (2012). Graphene oxide and its reduction: Modeling and experimental progress. *Sensors, 12*(9), 13720–13736. https://doi.org/10.3390/s120913720
49. Liang, Y., Li, Y., Wang, H., Zhou, J., Wang, J., Regier, T., & Dai, H. (2011). Co3O4 nanocrystals on graphene as a synergistic catalyst for oxygen reduction reaction. *Nature Materials, 10*(10), 780–786. https://doi.org/10.1038/nmat3087

50. Kim, H., Miura, Y., & Macosko, C. W. (2010). Graphene/polyurethane nanocomposites for improved gas barrier and electrical conductivity. *Chemistry of Materials, 22*(11), 3441–3450. https://doi.org/10.1021/cm100477v
51. Dresselhaus, M. S., & Dresselhaus, G. (2002). Intercalation compounds of graphite. *Advances in Physics, 51*(1), 1–186. https://doi.org/10.1080/00018730110113644
52. Lerf, A., He, H., Forster, M., & Klinowski, J. (1998). Structure of graphite oxide revisited. *The Journal of Physical Chemistry B, 102*(23), 4477–4482. https://doi.org/10.1021/jp9731821
53. Dreyer, D. R., Park, S., Bielawski, C. W., & Ruoff, R. S. (2010). The chemistry of graphene oxide. *Chemical Society Reviews, 39*(1), 228–240. https://doi.org/10.1039/B917103G
54. Pei, S., & Cheng, H. M. (2012). The reduction of graphene oxide. *Carbon, 50*(9), 3210–3228. https://doi.org/10.1016/j.carbon.2011.11.010
55. Eda, G., & Chhowalla, M. (2010). Chemically derived graphene oxide: towards large-area thin-film electronics. *Advanced Materials, 22*(22), 2392–2415. https://doi.org/10.1002/adma.200903689
56. Kumar, S., & Pareek, V. (2020). Recent advances in synthesis and applications of graphene–based nanocomposites for water purification. *Materials Research Express, 7*(3), 032003. https://doi.org/10.1088/2053-1591/ab63e6
57. Gao, W. (2015). The chemistry of graphene oxide. In D. R. Dreyer (Ed.), *Graphene oxide: Reduction recipes, spectroscopy, and applications* (pp. 61–95). Springer. https://doi.org/10.1007/978-3-319-15500-5_3
58. Hummers, W. S., & Offeman, R. E. (1958). Preparation of graphitic oxide. *Journal of the American Chemical Society, 80*(6), 1339. https://doi.org/10.1021/ja01539a017
59. Sharma, R. K., Ghose, R., & Rawat, R. S. (2020). Graphene oxide and its reduced forms for energy storage and environmental applications. *Current Science, 119*(4), 642–652.
60. Sadiq, M. M., Khan, T. A., & Ahmed, S. (2016). Controlled synthesis of graphene-based nanomaterials from petroleum residues for sustainable development. *Journal*

of Environmental Chemical Engineering, *4*(4), 4658–4666. https://doi.org/10.1016/j.jece.2016.08.012